EXPERIMENTAL ANALYSIS OF WAVE-INDUCED LOADS ON A CONTAINERSHIP IN MULTI-DIRECTIONAL SEA-STATES

S. DARRIGO[(1)], B. BOUSCASSE[(1)],G. DUCROZET[(1)]
F. BONNEFOY[(1)], G. de HAUTECLOCQUE[(2)]

solene.darrigo@ec-nantes.fr ; benjamin.bouscasse@ec-nantes.fr ; guillaume.ducrozet@ec-nantes.fr
felicien.bonnefoy@ec-nantes.fr ; guillaume.de-hauteclocque@bureauveritas.com

[(1)] Nantes Université, École Centrale Nantes, CNRS, LHEEA, UMR 6598, Nantes, France
[(2)] Bureau Veritas, Paris, France

I – Summary

Model-scale experiments in multi-directional waves are conducted with a 6750-TEU containership model at the wave tank of École Centrale Nantes. They were carried out following a previous experimental campaign in uni-directional waves. Combining the results from these campaigns allows for a comparison of experimental motions and internal loads with their linear theory prediction in uni-directional and multi-directional sea states. This paper focuses on the ship's Vertical Bending Moment (VBM) extreme response, which is one of the most important parameters for ship design. In particular, the VBM non-linear factor used by certification societies in their rule formulations, which are currently designed in uni-directional conditions, is compared to multi-directional cases.

II – Introduction

In the context of ship design, one crucial load to estimate is the vertical bending moment (VBM) corresponding to a 25-year return period. The long-term VBM statistics are derived from the short-term statistics of VBM response to single sea states and the long-term wave conditions. A sea state is defined by the power spectral density of the wave elevation, which is typically referred to as the wave spectrum. The long-term wave conditions are described with a wave scatter diagram, which shows the probability of occurrence of all the sea states that the ship may encounter during its lifetime. The short-term VBM response can be obtained with an experimental Monte Carlo approach, or with different numerical approaches, combining a hydrodynamic and a structural model applied in each sea state.

The linear hydrodynamic model is defined in the frequency domain. In this case, the VBM response spectrum and statistics are simply obtained from the Response Amplitude Operator (RAO) and the wave spectrum. However, in extreme wave conditions, non-linear effects render these models inaccurate and lead to under-prediction of extreme values. Unfortunately, non-linear models, defined in the time domain, can account for the non-linear behaviour but become quickly unreasonably time-consuming for ship design purposes. For instance, a time domain model that accounts for Froude-Krylov non-linearities and large motions [8] requires approximately a CPU time of one-tenth of the real-time. Thus, a 25-year return period would require 2.5 years of computation, which is impractical. Several methods have been developed to reduce the computational time required for time domain simulations, such as design sea state or design wave approaches. The design sea state approach [9] consists in only simulating the sea state contributing the most to the long-term response extreme. To reduce even more the computation time, the increased design sea state was developed with the idea of increasing the height of the considered sea state, so that the target extremes are reached more often. The objective of design wave approaches [3] is to simulate only a few waves that induce the target extreme response.

The structural model can represent either a rigid or flexible body, and provides the internal loads of the ship derived from the hydrodynamic loads.

To overcome the inaccuracy of linear models in extreme conditions, and the time requirements of non-linear models, certification companies have developed rule formulations for the marine industry. In order to assess the extreme non-linear loads, linear computations are corrected by a factor that accounts for the non-linear behaviour. This correction factor is called the non-linear factor, and is specified in

the rule formulations. For example, the non-linear factor for sagging (negative VBM values) from [13] is:

$$f_{nl,sag} = \max\left(1.0, 4.5\frac{1+0.2f_{bow}}{C_W\sqrt{C_B}L^{0.3}}\right) \tag{1}$$

with f_{bow} bow flare factor, C_W water plane coefficient in the loading condition, C_B block coefficient, and L rule length defined in [17]. The non-linear sagging moment is, in kN.m:

$$M_{w-sag} = -1.5f_R L^3 C C_W \left(\frac{B}{L}\right)^{0.8} f_{nl,sag} \tag{2}$$

at positions included in the interval $[0.35L; 0.55L]$ along the ship length from aft perpendicular, with f_R factor related to the operational profile, and C wave parameter. The rule formulations give formula for hogging (positive VBM values) as well.

To determine the non-linear factors, non-linear loads have to be assessed. This can be done numerically. However, there is a large variation between classification societies when comparing the non-linear vertical bending moment associated with a 25-year return period [10]. Therefore, the numerical determination of the non-linear factor is not straightforward, and its estimation should be confronted with experimental results. An experimental database has been built for uni-directional waves during what is referred as the BV2 campaign [15], and non-linear factors were extracted for a zero-speed 6750-TEU container-ship model. The design sea state with increased wave height approach [9] was developed under the assumption that the correction factors do not depend on the significant wave height of the sea state. This assumption was found to be valid thanks to the BV2 campaign [15].

The same experimental model is used in this paper, in multi-directional waves, for what is called the BV3 campaign. Very few articles have been published about the effect of spreading on the non-linearities [8]. The database and the results will be used later in the development of CFD tools and design waves techniques for directional waves, providing a reference for assessing the accuracy of the codes. The focus of the article is on the vertical bending moment in multi-directional waves and the comparison with uni-directional results from [15].

III – Experimental set-up

III – 1 Problem description

The case study is depicted in Figure 1a, it consists of a ship in waves moored with 4 lines. The mooring lines are needed to compensate for the drift induced by the waves in the absence of propulsion. The speed considered by classification societies for the assessment of internal loads is 5 knots, which justifies the choice to carry out the tests without forward speed. Two reference frames are needed to track the body motion, a Galilean reference frame R_0 and a body-fixed frame R_b. Figure 1b shows the ship model of this paper during an experimental test.

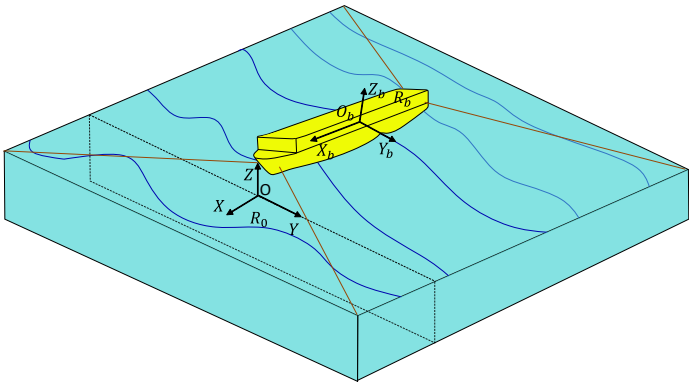

(a) Reference frames

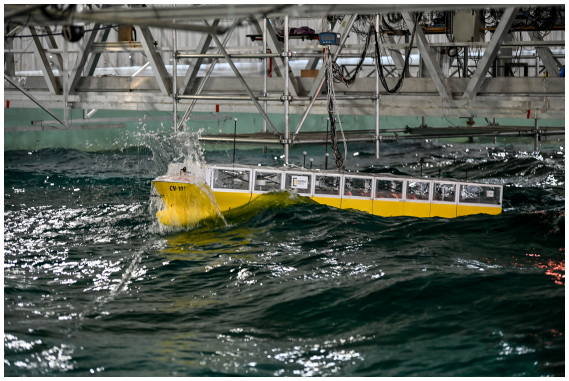

(b) Ship model in multi-directional waves

Figure 1: Illustration of case study of this paper

The architecture considered is shown in Figure 2: the hull is connected to the girder by pillars. To consider the internal loads, the ship can be decomposed into segments s_i composed of a beam part b_i and hull part h_i bounded between positions $[x_i, x_{i+1}]$ from the ship aft perpendicular (AP).

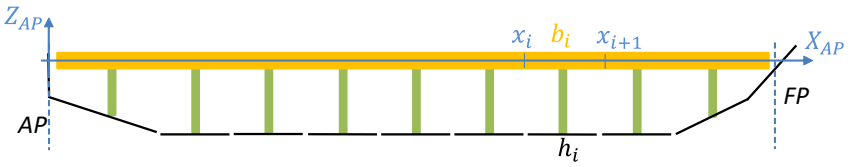

Figure 2: Internal ship architecture

III – 2 Ship geometry and loading conditions

The geometry used for the CN-101 model is the same as the benchmark [16]: a 1/65$^{\text{th}}$-scaled model of 6750-TEU containership shown in Figure 3 with the main properties given in Table 1. The CN-101 model was first used in the BV1 campaign done in regular head waves. The loading conditions and results of this campaign are given in [4].

Ship property	Full 1/1	Model CN-101 1/65
L_{pp} (m)	286.6	4.41
B_{wl} (m)	40	0.615
H (m)	24.2	0.372
T_m (m)	11.98	0.184
Displacement Δ	85724.7 t	312.152 kg
KG (m)	16.562	0.527
LCG from AP (m)	138.395	2.129
kxx (m)	14.4	0.222
kyy (m)	71.5	1.109
kzz (m)	71.4	1.106
Draft (m)	12.16	0.187

Table 1: General geometrical properties of 6750-TEU containership model

As detailed in [4], the ship is segmented into 9 parts shown in Figure 3, to study internal loads with the model of Figure 2. Each segment is composed of a girder part (grey), linked to a hull part (yellow) by a load cell. Segments 4 and 5 are linked by a load sensor called ATI. The location of the ATI sensor is intended to study the maximum vertical bending moment, as determined by [16].

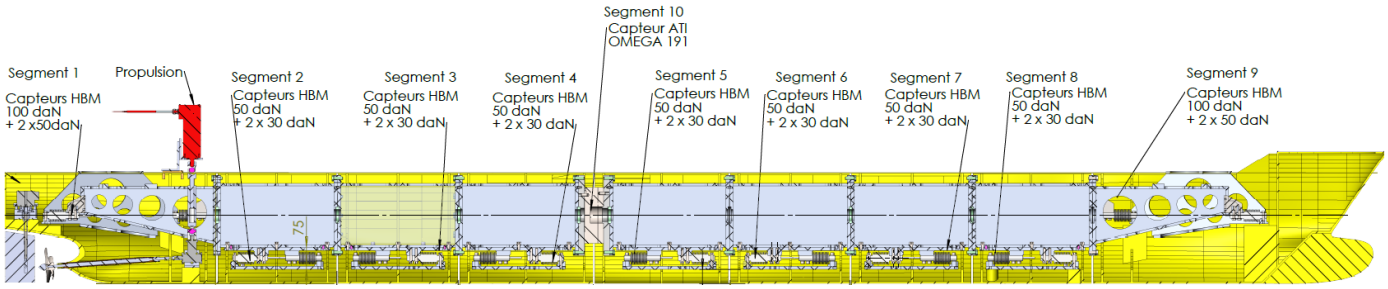

Figure 3: Ship segments

The details of each segment's properties, as reported in [14], are given in Table 2.

Segment	Mass (kg)	LCG (m)	KG (m)	x InterSeg from AP (m)	Ixx (kg.m^2)	Iyy (kg.m^2)	Izz (kg.m^2)	Ixz (kg.m^2)
Seg1	32.604	0.322	0.265	0.628	0.891	1.876	1.85	0.061
Seg2	28.713	0.827	0.252	1.038	1.487	1.47	1.029	−0.237
Seg3	26.195	1.242	0.206	1.448	0.718	0.72	0.869	0.002
Seg4	27.483	1.660	0.204	1.905	0.821	0.778	0.976	−0.07
ATI	31.634	1.905	0.252	-	0.3	0.191	0.191	0
Seg5	28.621	2.148	0.209	2.362	0.836	0.82	1.014	0.007
Seg6	37.503	2.565	0.291	2.772	1.715	1.553	1.065	−0.017
Seg7	35.006	2.996	0.283	3.182	1.41	1.363	1.017	0.165
Seg8	34.314	3.385	0.297	3.592	1.219	1.269	0.905	0.193
Seg9	29.852	3.957	0.280	4.587	0.557	1.863	1.896	0.041
Full model	311.925	2.146	0.257	-	10.616	383.317	381.864	−5.835

Table 2: Details of each segment main properties

III – 3 Instrumentation and acquisition

The sensors used on the model are:

- a 3 Degrees Of Freedom (DOF) load sensor between each segment composed of 3 HBM Z6FC3 load cells
- a 6-DOF load sensor ATI Omega 191 at its middle part
- an accelerometer ASC OS-325MF-PG placed on aft part
- an accelerometer at his front part
- an SBG IMU near amidships

The model is also instrumented with:

- 6 reflective markers to track the motions of the body with *Qualisys* cameras system
- on each mooring line, a tensiometer HBM U9C attached to the fairlead of the ship, and connecting the mooring lines to the ship model

The *Qualisys* software computes the centre of gravity (CoG) trajectory from the markers tracking. The coordinates of the markers are given in the body-referenced frame, with the CoG as the origin. The reference frame R_0 is defined through a calibration procedure.

Each sensor is connected to a *QuantumX* data acquisition module, and, if necessary, a conditioner. The modules send the collected data to computers through an Ethernet switch. A trigger signal from the wave-maker computer is sent to data acquisition computers to start or stop the acquisition. The sampling rate is set at 200 Hz for each sensor.

III – 4 Ship set-up and tank instrumentation

Figure 4 shows the model installed in the tank: 4 mooring lines connect the model to the tank walls, 9 resistive wave probes (WG) measure the wave elevation at different locations in the tank, 2 cameras record each test for real-time visualisation of the ship, and 4 cameras are used by Qualisys for body-tracking. (X, Y, Z) frame is a reference frame attached to the wave-maker.

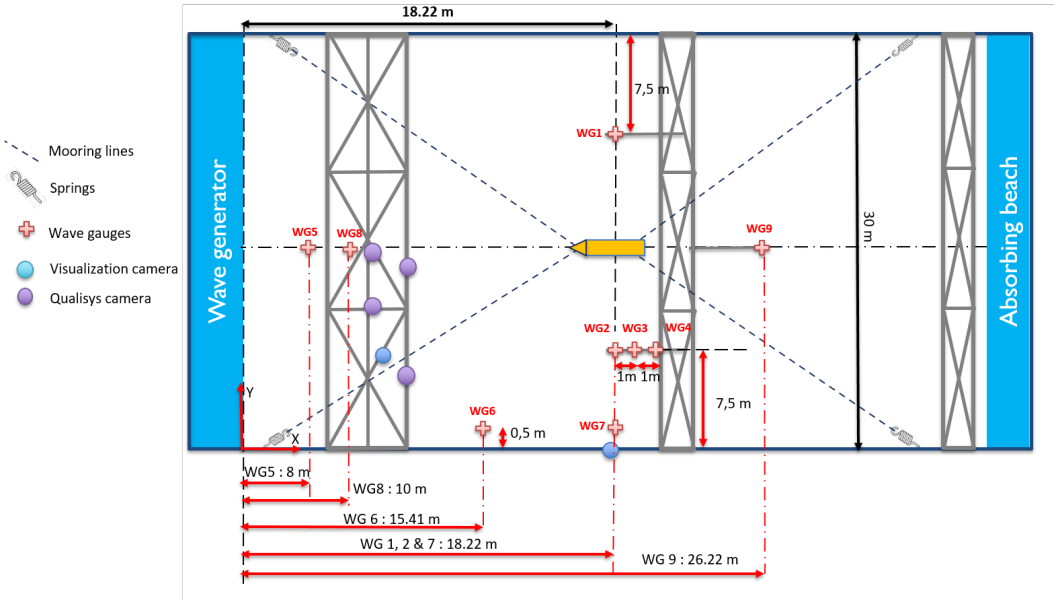

Figure 4: Tank instrumentation for body-tracking, visualisation and wave elevation measurements with moored ship

The stiffness of each mooring line spring is 58 N/m, their length at rest is 0.5 m, and their pre-tension is 13 N for lines 1 and 2, and 11 N for lines 3 and 4.

IV – Short-crested wave conditions and calibration

IV – 1 Test matrix

The tested directional wave conditions are given in Table 3. The target frequency spectrum $S_w(f)$ is of JONSWAP form [12], with H_s its significant wave height, T_p its peak period, and γ its form factor. We define $\theta = \left(\vec{X}_w, \vec{X}_b\right)$ as the wave heading, as shown Figure 5. The directional spreading function $D(\theta)$ is defined as the one found for extreme sea states over the North Atlantic main shipping routes [18]. It follows the form $D(\theta) = cos^s(\theta - \theta_m)$ with a mean direction $\theta_m = \pi$ (head waves) in the Qualisys reference frame (see Figure 5), and spreading factor $s = 3$. The directional spectrum is then $S_w(f, \theta) = S_w(f)D(\theta)$.

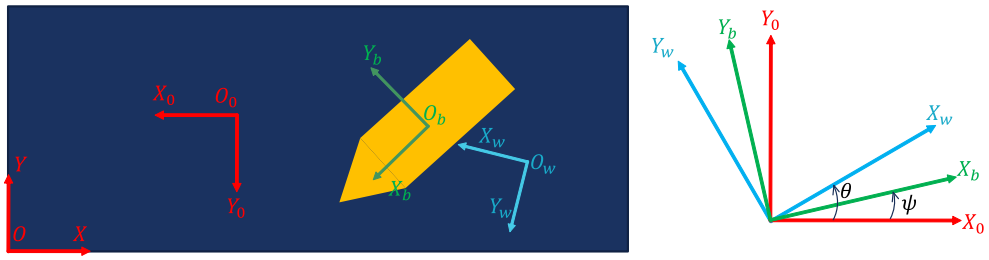

Figure 5: Wave-maker, Qualisys, body and wave frames (resp. with no index, index 0, b and w)

The tested sea states have a significant wave height at real-scale ranging from 6 m to 17 m, as it was shown in [1] that they are the most contributing sea states to extreme responses. Their steepness is increasing from SS6 to SS17. What we call a test is a random-phase realization of the sea surface elevation, lasting about 25 min. Between each test, there is a waiting time of 30 minutes to allow the tank free surface to return to calm water.

Sea state	H_s (m)	T_p (s)	γ	Number of tests	Analysis duration (h)	Number of waves	H_s/λ_p
SS6	0.0923	1.52	1	30	11	32989	2.6%
SS8	0.128	1.74	1.5	30	11.9	31131	2.6%
SS10	0.154	1.74	1.5	30	11.6	30336	3.3%
SS12	0.185	1.74	1.5	29	11.2	29081	3.9%
SS17	0.262	1.92	2.6	30	10.9	24819	3.8%

Table 3: Directional sea conditions tested at model-scale with $D(\theta) = cos^3(\theta - \pi)$ spreading

IV – 2 Wave calibration and measurement

A preliminary experimental campaign has been conducted without the model to assess the directional waves generated by the wave-maker. The tank set-up for the wave calibration and measurement is shown in Figure 6. The wave-maker is at $x = 0$ m. 19 wave probes are placed longitudinally at $y = 14.8$ m, and 8 transversely at $x = 18.2$ m. 2 directional networks of 7 probes are centred respectively at $(x = 13.50, y = 14.79)$ m for Network 1 and at model location $(x = 18.2, y = 14.86)$ m for Network 2. The right panel shows the shape of the networks: 3 probes are placed on a circle of radius 1 m and 3 others on a circle of radius 0.5 m, with another probe at the centre. The radius of $R = 1$ m and the shape of the directional networks are chosen from the results presented in [2] and [19].

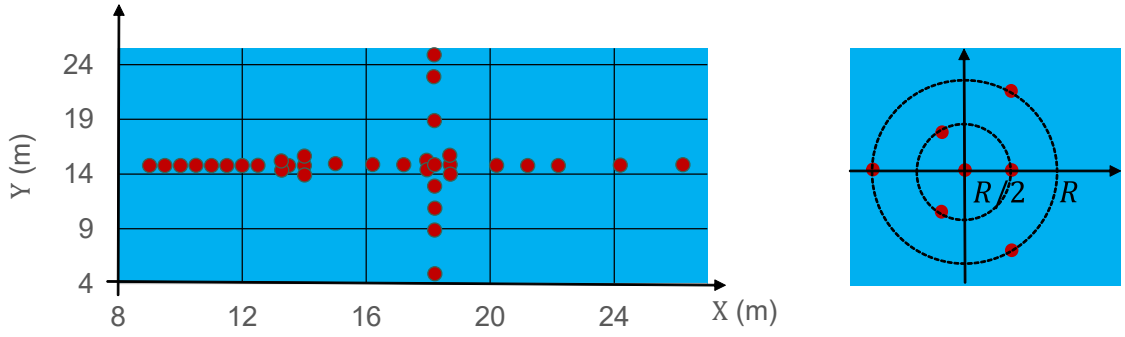

Figure 6: Full wave probes arrangement (left) and zoom on a directional network (right)

As a first step, the frequency spectrum $S_w(f)$ is measured at the model location and a frequency constant gain correction was applied to the wave-maker input to get a measured H_s close to the target one, and a measured frequency spectrum also close to the target one, see for instance Figure 7b.

In order to analyse the response of the ship to short-crested seas, it is necessary to define the directional wave spectrum $S(f, \theta)$ at the ship's location. The Extended Maximum Entropy Principle (EMEP) method, implemented by the open-source library *Diwasp* [7] as developed by [11], was used to compute directional spectra from two directional networks. Such a choice was justified from [2] and other reference articles from the literature, showing that EMEP is a good compromise between computational complexity and accuracy for stationary signals.

Segments of length $30T_p$ windowed by Blackmann-Harris method are used, with a 50% overlap for Welch computation of cross-spectra. $30T_p$ are used for FFT computation on each segment. 36 points are taken for directional discretisation between 0 deg and 360 deg. EMEP method has a maximum of 50 iterations. Note that the following results are given in $\mathcal{R}_w$ reference frame, as shown in Figure 5.

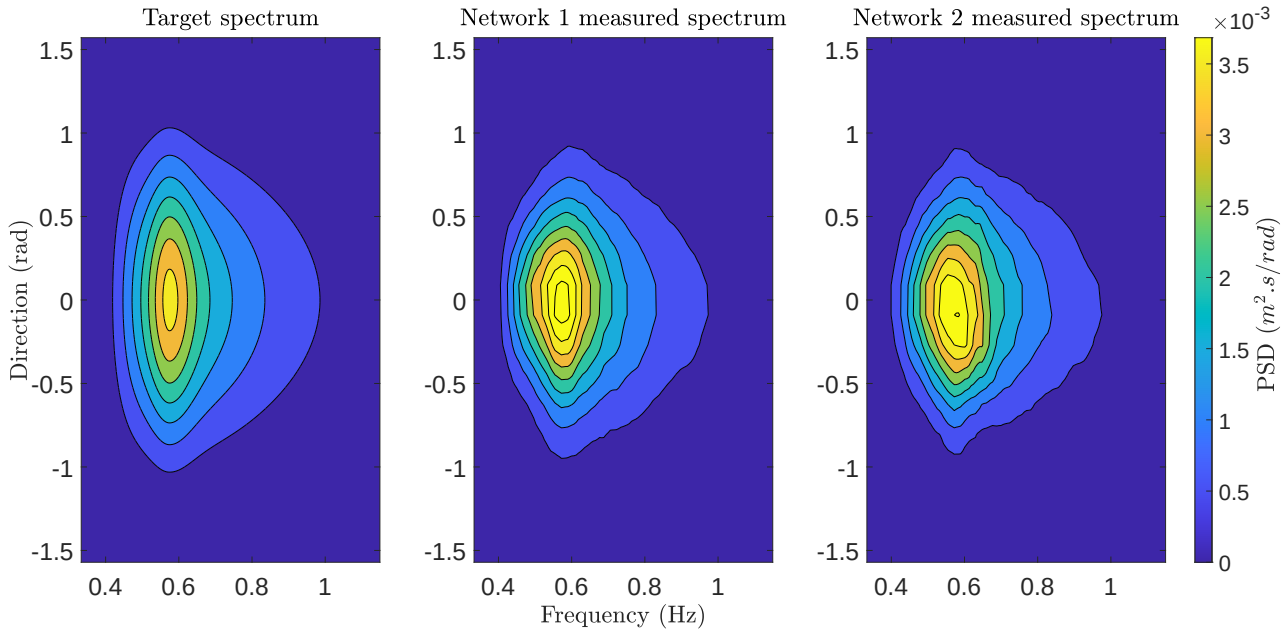

(a) Directional spectra

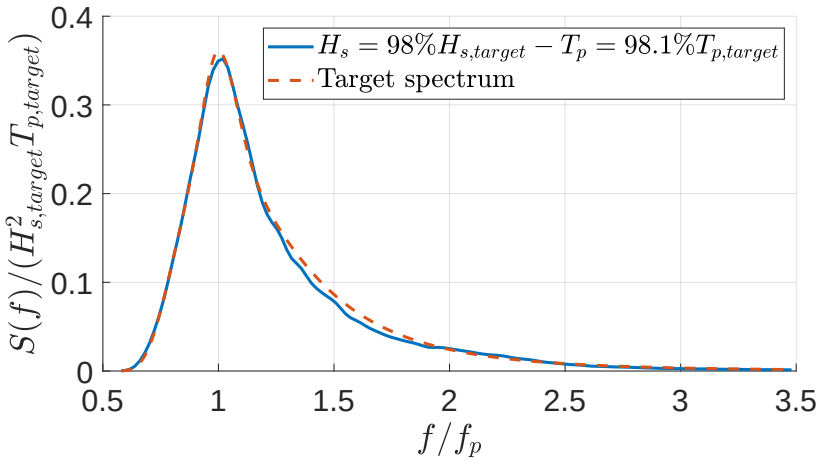

(b) Frequency spectrum at model position

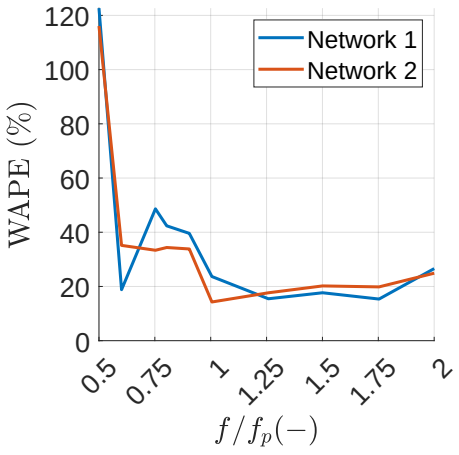

(c) $WAPE$ mode

Figure 7: Characterization of SS10

Figure 7 shows plots for the SS10 sea state characterization, as defined in Table 3. The target directional spectrum together with the measured directional spectra at Network 1 and Network 2 are shown in Figure 7a. The generated directional spectra appear close to the target one at both locations. For a more detailed comparison and to quantify the differences, Figure 7b compares the target and measured frequency spectra after calibration at the centre of Network 2. The relative difference with the target spectrum is 12% at the most in the frequency range $[0.75; 1.5]f_p$, reached at $1.4f_p$. The measured H_s is 98% of $H_{s_{target}}$ and measured T_p is 98.1% of $T_{p_{target}}$. Finally, Figure 7c shows the

Weighted Average Percent Error $WAPE$ on Network 1 and Network 2, defined as:

$$WAPE(f) = \frac{\int_0^{2\pi} |D_{\text{measured}}(\theta) - D_{\text{target}}(\theta)|\, d\theta}{\int_0^{2\pi} D_{\text{target}}(\theta) d\theta} \tag{3}$$

It allows for the quantitative estimation of the error on the directional spreading function $D(\theta)$. For this sea state, the error is 50% at $0.75 f_p$ and decreases to about 20% after f_p. Note that a previous study on synthetic linear multi-directional waves showed that the $WAPE$ of the EMEP method implemented for directional spectra estimation of SS10, with the same parameters and networks, was also around 20% after reaching convergence with about 150000 waves. This means that we cannot expect much lower $WAPE$ from the experimental data, and tends to indicate that the directional spreading function is correctly reproduced in the tank.

V – Influence of directional spreading on VBM response

The ATI sensor gives the torsion, maximum bending moments, and shear forces between segments 4 and 5 shown Figure 3. The values are given in the $\mathcal{R}_b$ reference frame. The selection of the analysis time window for each test is done manually. The starting time for the analysis is when the signal envelope of the reference WG2 wave probe (see Figure 4) is constant. Hence, the transient time is not taken for the analysis. For each test, the mean value of the 20 s time interval before the start of the wave-maker is removed from the analysis of the sensor signals, and is referred to as the calm water value.

V – 1 Probability of exceedance

To get the probability of exceedance (POE) for a time signal $s(t)$, a peak-over-threshold method is applied. The extreme events are obtained in each interval bounded by the up-crossings between the signal and its mean value. Crest M_i and trough m_i events are sorted with $M = [M_1, ..., M_i, ...M_n]$ containing crests by ascending order and $m = [m_1, ..., m_i, ...m_n]$ troughs by descending order, for n wave events. In our case, M and m arrays from all realisations of a single sea state are concatenated and sorted. The POE for an extrema e_i is then deduced from its rank in extrema array:

$$POE(e_i) = 1 - \frac{i}{n} \tag{4}$$

Jeffreys intervals based on [5], are used to get 95% confidence intervals for POE estimates.

Figure 8 shows the vertical bending moment POE obtained for SS6, SS10 and SS17 for uni-directional waves (BV2) and multi-directional waves (BV3). The scattered points are experimental values, and the solid lines show the above-mentioned confidence intervals.

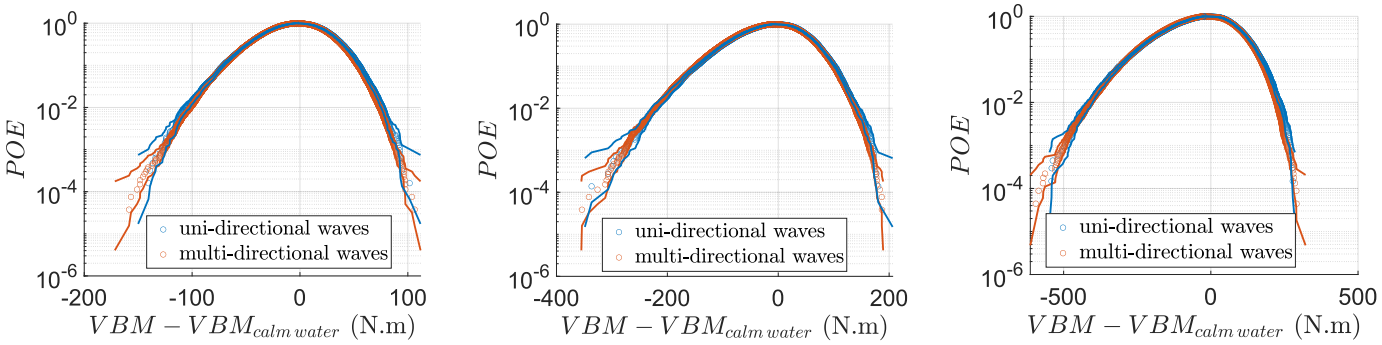

(a) SS6 (b) SS10 (c) SS17

Figure 8: VBM POE for uni-directional and multi-directional waves

For all sea states considered, there is no significant difference in the VBM POE between uni-directional and multi-directional waves. This is not intuitive, as the spreading is expected to reduce the energy focused on the ship model, hence making extreme values less probable. This result may not be generalisable and should be considered only for the specific configuration of this paper.

V – 2 Non-linear factor

V – 2.1 Definition

The input waves are considered linear if their free-surface elevation η is described by the random phase model, with N components as follows:

$$\eta(t) = \sum_{i=1}^{N} a_i \cos\left(2\pi f_i t + \phi_i\right) \tag{5}$$

with $(\phi_i)_{i\in[0,N]} \in [0, 2\pi]$ being random variables, described by an uniform law. The amplitude components a_i are determined from the power density spectrum S_w of η with:

$$a_i = \sqrt{2S_w(f_i)df} \tag{6}$$

In this linear model, η is considered Gaussian-distributed. We underline values which are complex representations: the complex representation of $x \in \mathbb{C}$ is $\underline{x} = |x| \exp\left(-j \arg(x)\right)$ with $j^2 = -1$. The linear response $\underline{VBM}_{lin}$ computed from the input wave elevation $\underline{\eta}$ is, at the frequency f_i:

$$\underline{VBM}_{lin}(f_i) = \underline{RAO}(f_i)\, a_i \exp(-j\phi_i) \tag{7}$$

Assuming a narrow-banded response frequency spectrum, the extrema of the linear VBM response $\max_t |VBM_{lin}(t)| := e_{lin}$ are then following a Rayleigh distribution given by:

$$POE(e_{lin}) = 1 - \exp\left(-\frac{e_{lin}^2}{2m_0}\right) \tag{8}$$

with m_0 the 0^{th}-order moment of the response spectrum defined as:

$$m_0 = \int_{\theta=-\pi}^{\pi} \int_{f=0}^{\infty} S_w(f,\theta)|RAO(f,\theta)|^2 df d\theta \tag{9}$$

The spectrum S_w used to calculate m_0 is the measured one. The RAO of the ship is computed with *Hydrostar*, a linear potential 3D Boundary Elements Method software [6]. m_0 and $POE(VBM_{lin,max})$ are then deduced. The non-linear factor f_{nl} is defined at a given POE level $POE = \hat{p}$ by:

$$f_{nl}(\hat{p}) = \frac{e_{lin}(\hat{p})}{e_{nl}(\hat{p})} - 1 \tag{10}$$

with e_{lin} the linear extremum value at the given $\hat{p}$, and e_{nl} the experimental (non-linear) extremum corresponding to the same POE. A particular attention is paid to compute 95% confidence intervals. To compute them, the linear POE curve is bounded, by taking into account m_0 statistical uncertainty on the series of realisations. The 95% confidence interval of m_0 is considered to be $\left[\bar{m}_0 \pm \alpha \frac{\sigma_{m_0}}{\sqrt{N_{tests}}}\right]$, with the bar notation being the mean value, σ the standard deviation, and α Student coefficient set to 1.96 for BV3 (30 samples) and 2.2 for BV2 (10 samples). In addition, the experimental POE is bounded by Jeffreys intervals.

V – 2.2 Results

RAO **computation** The mesh for the RAO computation contains about 2500 panels for half the hull (see Figure 9a), and the mass distribution from Table 2 is used for the computations. Figure 9b shows the RAO obtained with *HydroStar v8.14* together with the different frequency spectra tested experimentally (see Table 3).

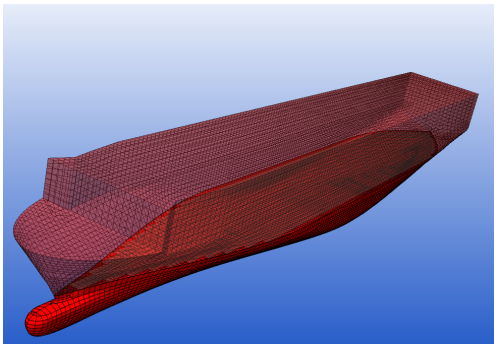

(a) Mesh used for RAO computation

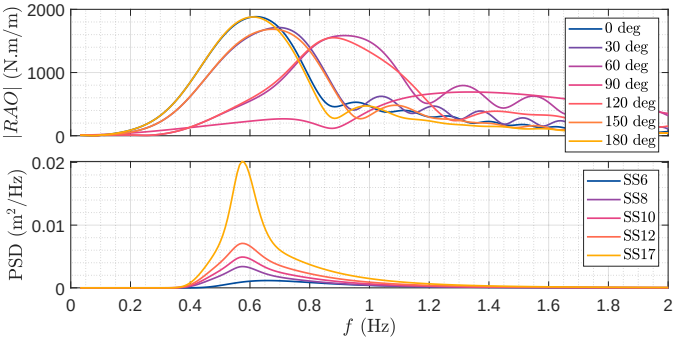

(b) Computed RAO and target frequency spectra for tested sea states

Figure 9: RAO linear calculation

Non-linear factors in uni-directional and multi-directional waves Figure 10 shows the experimental POE together with linear POE computed with m_0 estimates for SS6, SS10, SS17. As expected, the linear extremes (Rayleigh) are lower for multi-directional waves than uni-directional waves. In our case study, the experimental POE curves match for uni-directional and multi-directional waves.

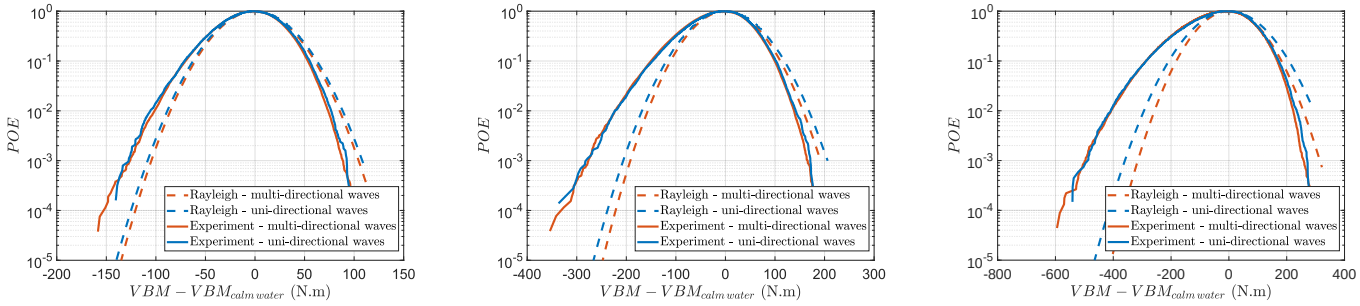

(a) SS6 (b) SS10 (c) SS17

Figure 10: Linear and experimental POE for SS6, SS10 and SS17

Such a variation of the linear POE can be explained by Figure 11, which shows the RAO at peak frequencies for SS6 to SS17, normalised by the uni-directional RAO.

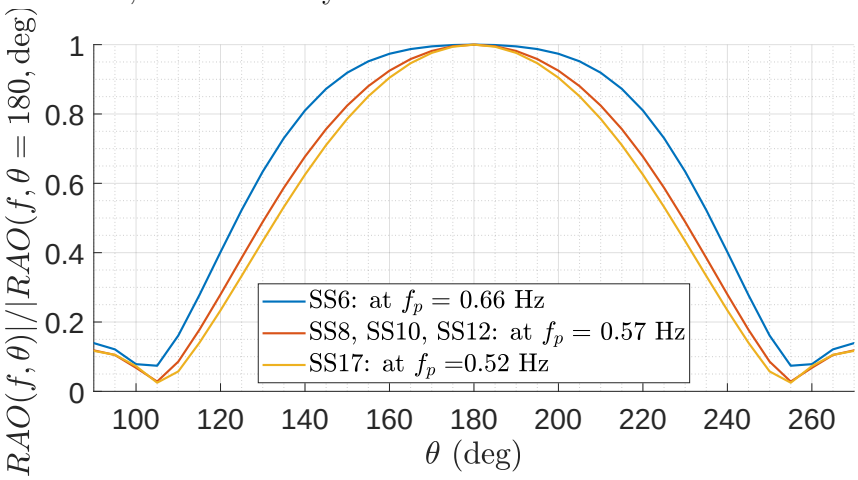

Figure 11: RAO at peak frequencies of SS6 to SS17

From this figure, it is clear that the effect of the spreading on the linear response varies between the sea states tested. When the heading deviates from 180 deg, the ratio $RAO(f,\theta)/RAO(f,\theta = 180\,deg)$ decreases, leading to a lower linear response in multi-directional waves than in uni-directional waves. The zeroth-order moment will decrease, as what can be predicted with equation 9. The computations give an increasing loss for m_0 between uni-directional to multi-directional waves for SS6 to SS17: 5% loss for SS6, 15% for SS8, SS10 and SS12, and 17% for SS17. The peak of $RAO(f,\theta)/RAO(f,\theta = 180,\ deg)$ becomes sharper from SS6 to SS17, leading to a VBM response more sensitive to the spreading: a smaller change of direction leads to a greater variations of the RAO ratio.

Figure 12 displays the non-linear factors for SS6, SS10 and SS17, combining uni-directional and multi-directionals plots. The non-linearities appear to be significantly greater from SS6 to SS17, especially for the sagging values. This is despite the fact that the experimental POE curves for unidirectional and multidirectional waves agree almost perfectly.

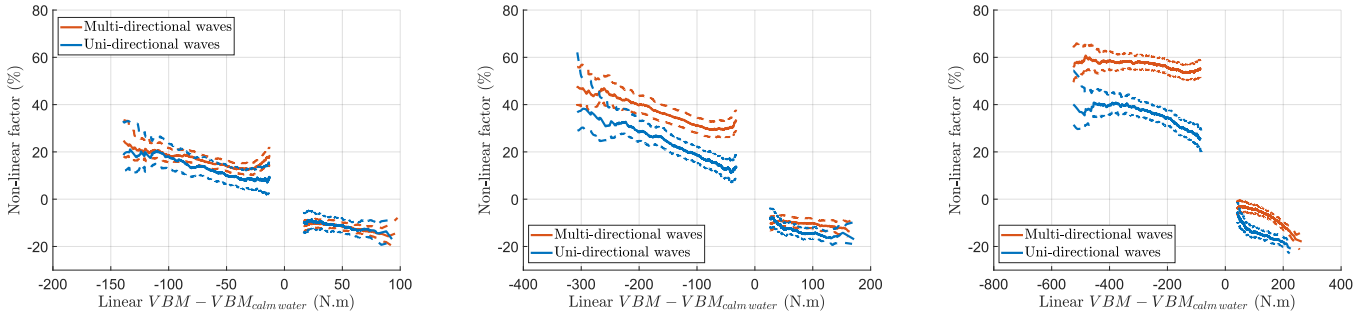

(a) SS6 (b) SS10 (c) SS17

Figure 12: Non-linear factors for SS6, SS10 and SS17

The fact that the experimental VBM POE do not vary between multi-directional and uni-directional waves is believed to be a coincidence. This is because the variation in the linear response is here almost perfectly offset by the variation in non-linear factors.

Figure 13a shows the non-linear factors for all sea states in uni-directional waves (results from [15]). The non-linear factors for hogging values match for all sea states, ranging from -10% to -20%. As for sagging values, the match occurs after 150 N.m approximately and lies between 10% to 40%. In this case, despite the small increase from SS6 to SS17, the non-linear factors depend mostly on the linear VBM on the tested sea states, as established in [15].

Figure 13b displays the non-linear factors obtained in multi-directional waves. The non-linear factors corresponding to hogging values range from -3% to -15%, which is close to the results obtained for uni-directional waves. Those corresponding to sagging values are between 20% and 60%, which goes much higher than for uni-directional waves. The non-linear factors for SS8, SS10, SS12 are similar for both hogging and sagging values. SS6 exhibits a greater absolute value for the sagging non-linear factor than the other sea states, and a lower one on hogging values. SS17 has the opposite trend. The influence of the spreading on the non-linear factor varies with the sea state, as discussed above with Figure 11. In the case of multi-directional waves, the spreading makes the non-linear factor sensitive to the sea state (T_p) under consideration.

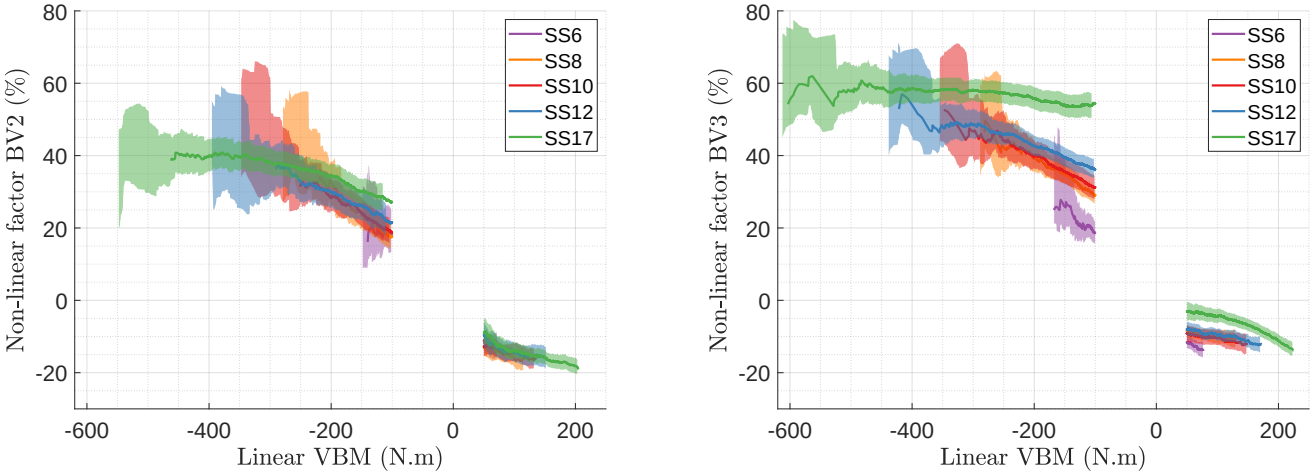

(a) Uni-directional waves (b) Multi-directional waves

Figure 13: Non-linear factors for all tested sea states

It has been shown that the spreading influences the non-linear factors. Indeed, the difference depends on the ship RAO and the sea state considered. Therefore, such a study has to be repeated when the ship properties and wave conditions are changed.

VI – Conclusion

Short-term Monte Carlo experiments were conducted to investigate the vertical bending moment response of a containership model submitted to extreme directional sea states of increasing steepness. The ship model is the same as the experimental campaign conducted by [15] in steep uni-directional irregular waves, allowing for comparison between results obtained in uni-directional and multi-directional waves. Sea states were characterised in wave-only tests. Target and measured uni-directional frequency spectra were compared, for wave calibration. WAPE values quantify the difference between the target and the measured directional spreading function. As in [15], the non-linear factor in uni-directional waves does not depend much on the sea state considered. It depends mostly on the linear value. Multi-directional tests showed that the non-linear factor of VBM response is influenced by the directionality of the waves, reaching much higher values for sagging in multi-directional waves. The values depend clearly on the spectrum shape of the sea state considered for multi-directional waves. On the cases studied in this paper, when comparing uni-directional and multi-directional sea states, the change in the non-linear ratio is almost perfectly compensated by the change in the linear response, resulting in a non-linear response POE that is almost the same. While the conclusion on the influence of the spreading has an effect on both the non-linear factors and linear responses is considered to be robust, the exact compensation is believed to be a coincidence. In addition to the results reported in this paper, the experimental database provides a valuable reference for benchmarking numerical approaches in extreme and multi-directional waves.

References

[1] H. N. Austefjord, G. de Hauteclocque, M. C. Johnson, and T. Y. Zhu. Update of wave statistics standards for classification rules. In *Advances in the Analysis and Design of Marine Structures*. CRC Press, 2023.

[2] M. Benoit. Extensive comparison of directional wave analysis methods from gauge array data. In *Extensive Comparison of Directional Wave Analysis Methods from Gauge Array Data*, pages 740–754, Jan. 1994.

[3] B. Bouscasse, A. Dermatis, S. Kim, G. Ducrozet, G. de Hauteclocque, and M. Lasbleis. Assessment of Nonlinear Loads and Motions Through Response Conditioned Design Waves: Practical Application and Limits. In *Assessment of Nonlinear Loads and Motions Through Response Conditioned Design Waves*, 2024.

[4] B. Bouscasse, A. Merrien, B. Horel, and G. de Hauteclocque. Experimental analysis of wave-induced vertical bending moment in steep regular waves. *Journal of Fluids and Structures*, 111:103547, May 2022.

[5] L. D. Brown, T. T. Cai, and A. DasGupta. Interval Estimation for a Binomial Proportion. *Statistical Science*, 16(2), May 2001.

[6] X.-B. Chen. Hydrodynamics in offshore and naval applications-part i. In *Keynote lecture of 6th Intl. Conf. HydroDynamics, Perth (Australia)*, 2004.

[7] C. O. Collins, H. Potter, B. Lund, H. Tamura, and H. C. Graber. Directional Wave Spectra Observed During Intense Tropical Cyclones. *Journal of Geophysical Research: Oceans*, 123(2):773–793, Feb. 2018.

[8] G. de Hauteclocque, Q. Derbanne, and T. Mienahou. Non Linearity of Extreme Vertical Bending Moment: Comparison of Design Wave Approaches and Short Term Approaches. In *Volume 9: Odd M. Faltinsen Honoring Symposium on Marine Hydrodynamics*, page V009T12A041, Nantes, France, June 2013. American Society of Mechanical Engineers.

[9] Q. Derbanne, F. Bigot, and G. de Hauteclocque. Comparison of Design Wave Approach and Short Term Approach With Increased Wave Height in the Evaluation of Whipping Induced Bending Moment. In *Volume 2: Structures, Safety and Reliability*, pages 299–308. American Society of Mechanical Engineers, 2012.

[10] Q. Derbanne, G. Storhaug, V. Shigunov, G. Xie, and G. Zheng. Rule formulation of vertical hull girder wave loads based on direct computation. In *Proceedings of the PRADS*, 2016.

[11] N. Hashimoto, T. Nagai, and T. Asai. Extension of the Maximum Entropy Principle Method for Directional Wave Spectrum Estimation. In *Coastal Engineering 1994*, pages 232–246, Kobe, Japan, Aug. 1995. American Society of Civil Engineers.

[12] K. Hasselmann, T. P. Barnett, E. Bouws, H. Carlson, D. E. Cartwright, K. Enke, J. A. Ewing, H. Gienapp, D. E. Hasselmann, P. Kruseman, A. Meerburg, P. Müller, D. J. Olbers, K. Richter, W. Sell, and H. Walden. Measurements of wind-wave growth and swell decay during the Joint North Sea Wave Project (JONSWAP). *Ergänzungsheft 8-12*, 1973.

[13] IACS. Unified requirement s11a - longitudinal strength standard for container ships. Technical report, IACS, 2015.

[14] S. Kim. *Experimental Study on Wave Bending Moments of a Zero-Speed Rigid Containership Model in Regular, Irregular, and Equivalent Design Waves*. PhD thesis, Ecole Centrale de Nantes, 2023.

[15] S. Kim, G. de Hauteclocque, B. Bouscasse, M. Lasbleis, and G. Ducrozet. Experimental analysis of extreme wave loads on a containership. *Ocean Engineering*, 306:118031, Aug. 2024.

[16] Y. Kim and J.-H. Kim. Benchmark study on motions and loads of a 6750-TEU containership. *Ocean Engineering*, 119:262–273, June 2016.

[17] I. Recommendation. Ur s2 rev2 cln. Technical report, IACS, 2019.

[18] I. Recommendation. Rec. no 34: Standard Wave Data. Rev. 2. Technical report, IACS, 2022.

[19] I. Young. On the measurement of directional wave spectra. *Applied Ocean Research*, 16(5):283–294, Jan. 1994.